Third International Conference on Inverse Design and Optimization in Engineering Sciences
(ICIDES-III) Editor: G.S.Dulikravich, Washington D.C. October 23-25, 1991.

ADJOINT OPERATOR APPROACH TO SHAPE DESIGN FOR INTERNAL INCOMPRESSIBLE FLOWS

H. Cabuk, C.-H. Sung*, and V. Modi,

Department of Mechanical Engineering,
Columbia University,
New York, New York 10027

* David Taylor Research Center
Bethesda, Maryland 20084

The problem of determining the profile of a channel or duct (given its upstream cross-section and length) that provides the maximum static pressure rise is solved. Incompressible, laminar flow governed by the steady-state Navier-Stokes equations is assumed. Recent advances in computational resources and algorithms have made it possible to solve the "direct" problem of determining such a flow through a body of known geometry. It is possible to obtain a set of "adjoint" equations, the solution to which permits the calculation of the direction and relative magnitude of change in the diffuser profile that leads to a higher pressure rise. The solution to the adjoint problem can be shown to represent an artificially constructed flow. This interpretation provides a means to construct numerical solutions to the adjoint equations that do not compromise the fully viscous nature of the problem. This paper addresses the algorithmic and computational aspects of solving the adjoint equations. The form of these set of equations is similar but not identical to the Navier-Stokes equations. In particular some issues related to boundary conditions and stability are discussed. The use of numerical solvers is validated by solving the problem of optimum design of a plane diffuser. The direct as well as the adjoint set of partial differential equations are discretized using a finite-volume formulation. Each of the resulting set of algebraic equations are then solved numerically to obtain a change in profile that will ensure an increase in the static pressure rise. Upon successive applications of this procedure, an "optimum" profile is obtained beginning with an initial guess of a diffuser profile. Such optimum diffuser profiles are obtained at Reynolds numbers varying from 10 to 2000. The optimality condition, that the shear stress all along the wall must vanish for the optimum diffuser, is also recovered from the analysis. It is shown that numerical solutions obtained in this fashion do satisfy the optimality condition.

1. INTRODUCTION

A shape optimization problem is one in which an objective function defined on a domain and/or on its boundary through the solution of a boundary value problem, is minimized (or maximized) with respect to the variation of the domain. One problem of this nature is "What is the shape of a body (of given volume) which has minimum drag when moved at constant speed in a viscous fluid?". Pironneau (1973) addressed this problem in Stokes flow for a three-dimensional unit-volume body. It was shown that at optimality the normal derivative of the velocity is constant along the boundary of the body. In addition it was also shown that the general shape of the body is similar to a prolate spheroid including a conical front end and rear ends of angle 120 degrees. However, due to the lack of a numerical Stokes flow solver, a complete body profile could not be obtained.

In a subsequent study, Pironneau (1974) derived the change in energy dissipation due to a small hump on a body in uniform, steady, laminar flow. Using the above result in conjunction with variational methods of optimal control "necessary optimality conditions" for four minimum-drag problems were obtained. These conditions lead to a set of equations for an additional set of variables called the "co-state" or the "adjoint" variables as opposed to the "direct" variables which are the unknown velocities. At the time Pironneau (1974) was unable to carry out such a numerical integration. Instead, however using a boundary layer assumption he was able to prove that a two-dimensional unit-area body with the smallest drag has a wedge-shaped

Third International Conference on Inverse Design and Optimization in Engineering Sciences
(ICIDES-III) Editor: G.S.Dulikravich, Washington D.C. October 23-25, 1991.

front end. In a subsequent work Glowinski and Pironneau (1975) presented numerical computations of the minimum-drag profile of a two-dimensional body in laminar flow, although with a Reynolds number large enough (between 1,000 to 100,000) to permit a boundary layer approximation. The present study belongs to this class in its theoretical approach with particular emphasis on computation of optimum profiles in the absence of simplifying assumptions such as Stokes flow or thin boundary layers.

Another related class of optimum design problems is the question of determining the profile of a two-dimensional body that will attain a desired surface pressure distribution. The body is assumed to be in otherwise uniform flow. The designer usually has a better understanding of how the performance is related to the the pressure distribution than the relationship between the profile and the performance. In recent survey paper, Jameson (1988) suggests that the design problem be treated as a control problem in which the control is the profile of the boundary. He also provides a comprehensive summary of the earlier related studies in this direction. In a significant step towards addressing real flows Giles et. al. (1985) addressed the problem of shape design for flows governed by the two-dimensional Euler equations. They write the two-dimensional Euler equations in a streamline coordinate system and for fixed pressure distribution obtain a Newton solution for the unknown surface coordinates.

In the present study optimum design of an internal flow component such as a diffuser in laminar flow is considered. The problem of determining the profile of a plane diffuser (of say, given upstream width and length) that provides the maximum static pressure rise is formulated using a variational method derived from optimal control theory. Careful consideration of the numerical stability of the adjoint equations we have been able to demonstrate the feasibility of optimum design in the context of laminar Navier-Stokes equations without the additional boundary layer assumption.

2. STATEMENT OF THE PROBLEM

Consider a plane diffuser as shown in figure 1 of given upstream width W_1 and given length L with incompressible, laminar flow through it. The flow is governed by the incompressible, steady forms of the Navier-Stokes and continuity equations. These are:

$$\begin{aligned} u_{i,i} &= 0 \\ u_j u_{i,j} &= -p^*_{,i} + \nu u_{i,jj} \end{aligned} \tag{1}$$

where $p^* = p/\rho$. Here u_i, p, ρ, and ν are the velocity components, pressure, density and kinematic viscosity respectively.

A no slip condition is imposed on the bounding wall. Dirichlet type boundary conditions are assumed at the entrance and exit, specifically, it is assumed that the streamwise velocity component at the entrance and exit is specified and the transverse velocity component at the entrance and exit is assumed to be zero. Symmetry conditions are assumed at the centerline. All velocities and lengths are scaled using the average entrance velocity, V, and the diffuser entrance width W_1 throughout the paper. Hence the Reynolds number for the flow through the diffuser is defined as $Re = (V \cdot W_1)/\nu$.

It is desired that the optimum diffuser profile be such as to maximize the value of this parameter for a given upstream width and length. Since pressure may vary across the diffuser inlet and exit regions it was decided to choose the change in the flow weighted integral (over the exit and inlet cross-sectional areas) of the static pressure rise as the objective function. This quantity is given by:

$$J(\Gamma_M) = \int_{\Gamma_I} p^* u_i n_i ds + \int_{\Gamma_O} p^* u_i n_i ds \tag{2}$$

where n_i is the i^{th} component of the unit normal vector and Γ_M is the portion of the diffuser wall that is to be shaped. The goal then is to determine the diffuser profile that maximizes the above function. The normalized diffuser length, L/W_1, (henceforth simply called the length) is kept constant. The normalized exit width W_2/W_1, (henceforth simply called the exit width) is left arbitrary, and its actual value for the optimum diffuser is part of the solution to the problem and is determined along with the rest of the profile. Since the only mechanism for total pressure drop in the diffuser is viscous dissipation, the optimum profile is also the profile for which the viscous dissipation is a minimum.

Third International Conference on Inverse Design and Optimization in Engineering Sciences
(ICIDES-III) Editor: G.S.Dulikravich, Washington D.C. October 23-25, 1991.

3. MATHEMATICAL FORMULATION

In this section, the variation of the objective function with respect to the variation of the boundary is obtained by means of a perturbation type of analysis. This analysis follows from arguments not unlike those used for optimum design in potential flow, in an earlier paper by Çabuk and Modi (1990).

First the variation of the solution of the direct problem due to boundary variation is obtained. Let $\rho(s)$ be an arbitrary function of arclength s, defined on Γ_M, and let ϵ be a positive number. Here Γ_M is part of the boundary that is to be shaped. The whole boundary, including the wall of the diffuser, the centerline and the inlet and exit areas, is denoted by Γ and the domain enclosed by Γ is denoted by Ω. Let each point on Γ_M be moved by $\epsilon\rho(s)$ along the outer normal direction. The curve constructed in this way is denoted by $\Gamma_{M,\epsilon}$ and the new domain is denoted by Ω_ϵ as shown in figure 1. Let $(u_i^\epsilon, p^\epsilon)$ be the solution of (1) in the new domain Ω_ϵ. Let (ϕ_i, π) be defined as follows.

$$\begin{aligned} \phi_i &= \lim_{\epsilon\to 0} \epsilon^{-1}\left[u_i^\epsilon - u_i\right] \qquad \in \Omega\,, \\ \pi &= \lim_{\epsilon\to 0} \epsilon^{-1}\left[p^\epsilon - p^*\right] \qquad \in \Omega\,. \end{aligned} \tag{3}$$

Then $(u_i^\epsilon, p^\epsilon)$ can be written as:

$$\begin{aligned} u_i^\epsilon &= u_i + \epsilon\phi_i \\ p^\epsilon &= p^* + \epsilon\pi \end{aligned} \tag{4}$$

Since both $(u_i^\epsilon, p^\epsilon)$ and (u_i, p^*) satisfy the Navier-Stokes equations, it can be shown that (ϕ_i, π) satisfy the following set of equations:

$$\begin{aligned} \phi_{i,i} &= 0 \\ u_j\phi_{i,j} + \phi_j u_{i,j} &= -\pi_{,i} + \nu\phi_{i,jj} \end{aligned} \tag{5}$$

In a similar way it can be shown that on the fixed portions of the boundary

$$\phi_i = 0 \qquad \text{on } (\Gamma - \Gamma_M) \tag{6}$$

since both u_i^ϵ and u_i satisfy the same boundary conditions.

The next step is to derive the conditions satisfied by ϕ_i on Γ_M. Consider a point P on Γ_M, and a corresponding point P_ϵ on $\Gamma_{M,\epsilon}$ such that P_ϵ lies on the outward normal $\vec{n}$, as shown in figure 1. Assume that $\epsilon\rho(s)$ is positive. A Taylor's series expansion of u_i^ϵ about the point P, evaluated at $\bar{x} = \bar{x}|_{P_\epsilon}$, along the normal direction $\vec{n}$ is

$$\begin{aligned} u_i^\epsilon]_{P_\epsilon} &= u_i^\epsilon]_P + \epsilon\rho\left(\frac{\partial u_i^\epsilon}{\partial n}\right)_P + O(\epsilon^2) \\ &= u_i]_P + \epsilon\phi_i]_P + \epsilon\rho\left(\frac{\partial u_i}{\partial n}\right)_P + O(\epsilon^2) \end{aligned} \tag{7}$$

Since the velocities satisfy the no slip condition on Γ_M, (i.e. $u_i^\epsilon]_{P_\epsilon} = u_i]_P = 0$);

$$\phi_i = -\rho\left(\frac{\partial u_i}{\partial n}\right) \qquad \text{on } \Gamma_M. \tag{8}$$

The first variation of the objective function is obtained next. The value of the objective function for the new domain is given by,

$$J(\Gamma_{M,\epsilon}) = \int_{\Gamma_I} p^\epsilon u_i^\epsilon n_i ds + \int_{\Gamma_O} p^\epsilon u_i^\epsilon n_i ds \tag{9}$$

The first variation of the objective function, δJ, is defined by the relation

$$J(\Gamma_{M_\epsilon}) - J(\Gamma_M) = \epsilon\delta J + O(\epsilon^2)\,. \tag{10}$$

The first variation of the objective function can be shown to be:

$$\delta J = \int_{\Gamma_I} \pi u_i n_i ds + \int_{\Gamma_O} \pi u_i n_i ds\,, \tag{11}$$

Third International Conference on Inverse Design and Optimization in Engineering Sciences
(ICIDES-III) Editor: G.S.Dulikravich, Washington D.C. October 23-25, 1991.

which is an integral expression over the entrance and exit boundaries. The next step is the transformation of this integral from one that is over Γ_I and Γ_O to one that is over Γ_M. This is achieved through the introduction of an adjoint variable problem. The inner product of the perturbation equations (5) and the adjoint variables, (z_i, r), integrated over the domain, and added to (11), and after using the divergence theorem gives

$$\begin{aligned}\delta J = &\oint \pi\,(u_i - z_i)\,n_i ds + \nu \oint \left(z_i \frac{\partial \phi_i}{\partial n} - \phi \frac{\partial z_i}{\partial n}\right) ds \\ &+ \oint \left(r\phi_i n_i - \phi_i z_i u_j n_j - u_i z_i \phi_j n_j\right) ds + \iint \pi z_{i,i} dA \\ &+ \iint \phi_i \left(\nu z_{i,jj} + u_j z_{i,j} + u_j z_{j,i} - r_{,i}\right) dA\ .\end{aligned} \tag{12}$$

The adjoint problem has to be defined such that the domain integrals in (15) vanish identically. The choice of boundary conditions for these equations is made such that the only nonzero terms are those that are integrals over Γ_M, the wall that is to be shaped. Let us define the following adjoint problem

$$\begin{aligned} z_{i,i} &= 0 && \text{in } \Omega \\ \nu z_{i,jj} + u_j(z_{i,j} + z_{j,i}) - r_{,i} &= 0 && \text{in } \Omega \\ z_i &= u_i && \text{on } \Gamma. \end{aligned} \tag{13}$$

Using (6), (8), and (13), equation (12) can be written as

$$\delta J = \nu \int_{\Gamma_M} \rho(s) \left(\frac{\partial u_i}{\partial n}\right) \left(\frac{\partial z_i}{\partial n}\right) ds\ . \tag{14}$$

In the above equation, the integration is over the boundary that is to be shaped. We can choose $\rho(s)$ as:

$$\rho(s) = \omega(s) \left(\frac{\partial u_i}{\partial n}\right) \left(\frac{\partial z_i}{\partial n}\right) \tag{15}$$

since that would ensure a positive change in the objective function, J, for a sufficiently small non-negative weighting function, $\omega(s)$. The function $\rho(s)$ provides the boundary movement for a positive change in J. To evaluate $\rho(s)$ we need to solve the direct problem (i.e. Navier-Stokes equations) given by (1) and the adjoint problem in z_i given by (13). Note that the optimality condition is satisfied when either the shear stress, $\partial u_i/\partial n$, or the adjoint shear stress, $\partial z_i/\partial n$, on the walls vanishes. The former criterion for optimum diffuser profiles was also pointed out by Chang(1976).

It will be shown that the above formulation is equivalent to the earlier work of Glowinski and Pironneau (1975). By a change of variable, the adjoint problem can be transformed into the following form:

$$\begin{aligned} w_{i,i} &= 0 && \text{in } \Omega \\ \nu w_{i,jj} + u_j w_{i,j} + w_j u_{j,i} - q_{,i} &= -u_j u_{i,j} && \text{in } \Omega \\ w_i &= 0 && \text{on } \Gamma. \end{aligned} \tag{16}$$

where $2w_i = (z_i - u_i)$ and $2q = \left(r - p^* + (1/2)u_j^2 - 2u_j w_j\right)$. The first variation of the objective function then becomes

$$\delta J = \nu \int_{\Gamma_M} \rho \left(\frac{\partial u_i}{\partial n}\right) \left(\frac{\partial u_i}{\partial n} + 2\frac{\partial w_i}{\partial n}\right) ds\ . \tag{17}$$

The form of the adjoint variable problem defined by (16) is identical to that derived by Glowinski and Pironneau (1975). Either one of the above adjoint problems can be solved numerically to obtain the next shape. However upon examination of (16), it becomes evident that the $w_j u_{j,i}$ term may lead to a numerically unstable scheme. This is because the approach to steady state would be attained via an iterative "time evolution" like scheme that would then be of the form $dw/dt = w(\text{const}) + \cdots$. This form is likely to result in the exponential growth of the inevitable roundoff and truncation errors present at any iterative step. Also

Third International Conference on Inverse Design and Optimization in Engineering Sciences (ICIDES-III) Editor: G.S.Dulikravich, Washington D.C. October 23-25, 1991.

the presence of the inhomogeneous term, $-u_j u_{i,j}$, in the above equations may lead to a linear growth of the roundoff and truncation errors in the numerical computations. It is expected that these numerical difficulties will be absent in the (z_i, r) formulation of the adjoint variable problem obtained in this paper and given by (13). Hence this is the set of equations for which the algorithm for the numerical solution of the adjoint problem is developed.

As pointed out by Pironneau (1974), the adjoint equations do not seem to arise from any identifiable physical phenomenon. It is however possible to demonstrate that the adjoint variable problem is associated with a certain artificially constructed flow. A change of variables leads to the following form.

$$\begin{aligned} z'_{i,i} &= 0 && \text{in } \Omega \\ \nu z'_{i,jj} - u'_j \left(z'_{i,j} + z'_{j,i}\right) - r'_{,i} &= 0 && \text{in } \Omega \\ z'_i = u'_i &= -u_i && \text{on } \Gamma. \end{aligned} \tag{18}$$

where $z'_i = -z_i$, $u'_i = -u_i$, and $r' = -r$. The first equation in (18) is identical to the continuity equation. Compare the second equation in (18) with the Navier-Stokes equation written here in a slightly different form.

$$\nu u_{i,jj} - u_j \left(u_{i,j} + u_{j,i}\right) - \tilde{p}_{,i} = 0 \tag{19}$$

where $\tilde{p} = p^* - (1/2)u_k^2$. Observe that the problem in adjoint variable z'_i is analogous to the the Navier-Stokes problem in variable u_i with the following exception: the convective velocities in the adjoint problem are specified rendering the problem linear and are obtained from the direct problem. These convective velocities, u'_i, are identical in magnitude but opposite in direction to those of the "direct" problem. The boundary conditions for the adjoint variables are $z'_i = -u_i$ on Γ. Hence on the walls they imply a no slip condition as in the direct problem. But at the inflow and outflow boundaries, "adjoint" flow is found entering at the domain exit Γ_O and leaving at the domain entrance Γ_I, thus suggesting an "adjoint" flow in the direction opposite to that of the actual flow.

The above interpretation of the adjoint variable problem will be useful in constructing a modified problem whose solution will provide numerical values, albeit approximate, for the shear stress, $\partial u_i/\partial n$, and the adjoint shear stress, $\partial z_i/\partial n$, in (15). It is found that a shape optimization algorithm that obtains its boundary movement from these approximate numerical solutions does indeed lead to diffuser shapes that satisfy the optimality condition.

4. NUMERICAL ASPECTS

The boundary conditions chosen for the diffuser in the above formulation are of Dirichlet type. A parallel flow of arbitrary distribution is assumed to exist at the diffuser entrance and exit. These boundary conditions are clearly unrealistic both from a practical as well as computational standpoint. However this is the only set of boundary conditions for which we have been able to derive the adjoint variable problem. Given this limitation it was decided to verify whether the boundary movement suggested by (15) would continue to provide a means to obtain optimum shapes even if some of the Dirichlet conditions were replaced with computationally suitable Neumann conditions.

Boundary Conditions for Navier-Stokes Equations

A parallel flow assumption at the upstream boundary implies Dirichlet boundary conditions for both the velocity components. Instead a computationally desirable Neumann condition for the transverse velocity component ($\partial u_2/\partial n = 0$ on Γ_I) is substituted while retaining a Dirichlet condition for the streamwise component. A parabolic profile corresponding to a fully developed laminar flow is specified for this component. At the downstream boundary the parallel flow assumption is replaced with computationally desirable Neumann conditions for both the velocity components ($\partial u_1/\partial n = \partial u_2/\partial n = 0$ on Γ_O). Similar approximations will be made in the solution of the adjoint variable problem, keeping in mind the reversal of the role of entrance and exit boundaries. At the solid wall, a boundary whose profile is to be determined, a no slip condition is enforced. At the diffuser centerline the usual symmetry conditions are used since the flow is assumed to be symmetric. At the entrance, exit, and wall, pressure has been extrapolated from the within the domain by assuming that the second derivative of the pressure vanishes on the domain boundary. At the centerline symmetry condition is imposed for the pressure.

Third International Conference on Inverse Design and Optimization in Engineering Sciences (ICIDES-III) Editor: G.S.Dulikravich, Washington D.C. October 23-25, 1991.

Boundary Conditions for Adjoint Equations

The role of entrance and exit are reversed for the adjoint equations. Therefore, at the exit boundary a Dirichlet type condition is used only for the streamwise component of the co-state vector. Therefore we set $z_1 = u_1$ on Γ_O, with u_1 taken from the solution of the Navier-Stokes equations. For the remaining component z_2 of the co-state vector at exit and for both components of the co-state vector at entrance, Neumann conditions are employed instead. At the wall where all velocity components vanish and therefore, z_i, the co-state vector that is analogous to the velocity is set to zero. The adjoint variable, r^*, is analogous to the pressure term in the Navier-Stokes equations and hence no analytical boundary condition is available for this variable. However, a computational boundary condition is implemented for this variable. The value of r^* is extrapolated to the boundary from values at interior points assuming that the streamwise second derivative vanishes at the boundary. This is done at all boundaries except at the centerline where a symmetry condition is enforced.

5. NUMERICAL SOLVERS

Navier-Stokes Equations Solver

The primitive variable form of the incompressible steady Navier-Stokes equations is solved using an artificial compressibility formulation due to Chorin(1967). In this formulation, the continuity equation is modified using the time derivative of the pressure term. The steady-state solution of the Navier-Stokes equations is then obtained as the large time solution of the unsteady momentum equations with the perturbed divergence equation. These unsteady equations are:

$$\begin{aligned} p^*_t + \beta^2 u_{i,i} &= 0 \\ u_{i,t} + (u_j u_i)_{,j} &= -p^*_{,i} + \nu u_{i,jj} \end{aligned} \tag{20}$$

where β is analogous to the speed of sound. Note that these equations do not represent any transient physical phenomenon and hence the transient solution has no physical meaning until steady state is attained. This is indicated by the vanishing of the time derivative terms in the numerical solution.

The equations are normalized using the velocity and length scales V and W_1 defined earlier. In addition time and pressure are normalized using the ratio W_1/V and ρV^2 respectively. The Reynolds number of the flow through the diffuser is then given by $Re = (V \cdot W_1)/\nu$.

The equations are discretized in space using a finite volume formulation. The spatial discretization is performed on the conservative form of the governing equations using a central difference scheme.

An explicit one-step multistage Runge-Kutta stepping scheme is used for integration in time. Since transient behavior is not an issue and a larger time step is desirable, a four-stage Runge-Kutta scheme with first order accuracy in time and a relatively high Courant-Friedrichs-Lewy (CFL) number has been chosen. In order to improve the convergence rate, a local time step is computed for each cell at each elapsed time level. These time steps have been estimated from a stability analysis of the algorithm. A fourth order linear artificial dissipation term is introduced to damp the high-frequency oscillations associated with the so-called sawtooth or plus-minus waves, i.e. waves associated with the shortest wavelengths. Implicit residual smoothing is performed at each iteration to enhance the stability region of the technique. A more complete discussion of the finite volume formulation, stability considerations, local time stepping, artificial dissipation, implicit residual smoothing and the computational boundary conditions is provided in Cabuk, Sung and Modi (1991).

The computational grid is generated by solving a set of elliptic partial differential equations similar to those suggested by Thompson et al. (1974). The set of algebraic equations thus obtained is solved by successive over-relaxation (SOR). A typical grid is shown in figure 2. Grids generated by this method were nearly orthogonal and the cell dimensions in each direction are approximately equal.

Adjoint Equation Solver

The solution to the adjoint set of equations is obtained as the steady state solution to the following set of equations:

$$\begin{aligned} r^*_t &= -\beta^2 z_{i,i} \\ z_{i,t} &= \nu z_{i,jj} + u_j(z_{i,j} + z_{j,i}) - \frac{1}{2}(z_k z_k)_{,i} - r^*_{,i} \end{aligned} \tag{21}$$

Third International Conference on Inverse Design and Optimization in Engineering Sciences (ICIDES-III) Editor: G.S.Dulikravich, Washington D.C. October 23-25, 1991.

where $r^* = r - z_k z_{k,i}$. A nonlinear term $\frac{1}{2}(z_k z_k)_{,i}$ is introduced in the above equation to enhance the rate of convergence. The utility of this term was established by means of preliminary calculations performed on a straight duct geometry where an exact solution of the Navier-Stokes solution is known for fully developed laminar flow.

The equations are normalized following a procedure similar to that utilized for the Navier-Stokes equations. The nondimensional form of the above equation is identical to the equations above with the exception of the first term on the right hand side of (21) where the kinematic viscosity, ν, is replaced by the reciprocal of the Reynolds number.

The numerical algorithm for the solution of the adjoint set of equations is essentially similar to the algorithm for the Navier-Stokes equations. Some subtle but important differences do exist since the equations solved are after all not the same. A discussion of the numerical algorithm is presented here, since this solution to the best of our knowledge represents the first successful numerical solution of the adjoint set of equations in the absence of either a thin boundary layer or a Stokes flow assumption. Spatial discretization is carried out by centered-difference finite volume formulation. The term, $u_j(z_{i,j} + z_{j,i})$, on the right hand side of (21) is not in a divergence form. In the treatment of this term the velocities, u_j, which have already been obtained by the Navier-Stokes solver, are treated as known quantities and are assumed constant inside each cell. Hence the volume integral over the cell is performed by applying the divergence theorem to the remaining part of this term, i.e. $(z_{i,j} + z_{j,i})$.

The other terms in (21) are treated in the same fashion as the finite volume formulation of the Navier-Stokes equations. A fourth order linear artificial dissipation term is introduced to damp high-frequency oscillations. Time integration is carried out by a Runge-Kutta scheme with local time stepping. The discrete form of the equations for the adjoint problem are:

$$\Delta V \frac{dq}{dt} - (A\delta_I + B\delta_J + C\delta_K)q = E\frac{Re^{-1}}{\Delta V}(SI\delta_I^2 + SJ\delta_J^2 + SK\delta_K^2)q - \epsilon K(\delta_I^4 + \delta_J^4 + \delta_K^4)q \qquad (22)$$

where

$$A = \begin{bmatrix} 0 & \beta^2 SIX & \beta^2 SIY & \beta^2 SIZ \\ SIX & U + (u_1 - z_1)SIX & (u_1 - z_1)SIY & (u_1 - z_1)SIZ \\ SIY & (u_2 - z_3)SIX & U + (u_2 - z_2)SIY & (u_2 - z_2)SIZ \\ SIZ & (u_3 - z_3)SIX & (u_3 - z_3)SIY & U + (u_3 - z_3)SIZ \end{bmatrix}$$

$$B = \begin{bmatrix} 0 & \beta^2 SJX & \beta^2 SJY & \beta^2 SJZ \\ SJX & V + (u_1 - z_1)SJX & (u_1 - z_1)SJY & (u_1 - z_1)SJZ \\ SJY & (u_2 - z_3)SJX & V + (u_2 - z_2)SJY & (u_2 - z_2)SJZ \\ SJZ & (u_3 - z_3)SJX & (u_3 - z_3)SJY & V + (u_3 - z_3)SJZ \end{bmatrix}$$

$$C = \begin{bmatrix} 0 & \beta^2 SKX & \beta^2 SKY & \beta^2 SKZ \\ SKX & W + (u_1 - z_1)SKX & (u_1 - z_1)SKY & (u_1 - z_1)SKZ \\ SKY & (u_2 - z_3)SKX & W + (u_2 - z_2)SKY & (u_2 - z_2)SKZ \\ SKZ & (u_3 - z_3)SKX & (u_3 - z_3)SKY & W + (u_3 - z_3)SKZ \end{bmatrix}$$

$$E = \begin{bmatrix} 0 & 0 & 0 & 0 \\ 0 & 1 & 0 & 0 \\ 0 & 0 & 1 & 0 \\ 0 & 0 & 0 & 1 \end{bmatrix}$$

and

$$q = [r^*, z_1, z_2, z_3]^T$$

with

$$U = u_1 SIX + u_2 SIY + u_3 SIZ, \qquad SI = SIX^2 + SIY^2 + SIZ^2,$$
$$V = u_1 SJX + u_2 SJY + u_3 SJZ, \qquad SJ = SJX^2 + SJY^2 + SJZ^2,$$
$$W = u_1 SKX + u_2 SKY + u_3 SKZ, \qquad SK = SKX^2 + SKY^2 + SKZ^2$$

Third International Conference on Inverse Design and Optimization in Engineering Sciences
(ICIDES-III) Editor: G.S.Dulikravich, Washington D.C. October 23-25, 1991.

The volume of the cell is ΔV and (SIX, SIY, SIZ), (SJX, SJY, SJZ) and (SKX, SKY, SKZ) are the surface-area vectors normal to the I, J and K cell surfaces, respectively. SI, SJ and SK are the squares of the surface areas of I, J and K cell surfaces, respectively. The first, second and fourth order centered differences are defined in the same fashion as in Sung(1987). The maximum local time step permitted for stability is obtained by neglecting both the viscous and the artificial dissipation terms in the adjoint problem and is given by

$$\Delta t \leq CFL\left(\frac{\Delta V}{\lambda_0}\right) \tag{23}$$

The maximum eigenvalue, λ_0, in the above equation is estimated as

$$\lambda_0 = \frac{1}{2}\left[\hat{U} + \sqrt{\hat{U}^2 + \beta^2 C^2}\right] \tag{24}$$

where

$$\begin{aligned}\hat{U} = &|U| + |SIX\,(u_1 - z_1)| + |SIY\,(u_2 - z_2)| + |SIZ\,(u_3 - z_3)| \\ &+ |V| + |SJX\,(u_1 - z_1)| + |SJY\,(u_2 - z_2)| + |SJZ\,(u_3 - z_3)| \\ &+ |W| + |SKX\,(u_1 - z_1)| + |SKY\,(u_2 - z_2)| + |SKZ\,(u_3 - z_3)|\end{aligned}$$

and

$$\begin{aligned}C^2 = &(|SIX| + |SIY| + |SIZ|)^2 \\ &+(|SJX| + |SJY| + |SJZ|)^2 \\ &+(|SKX| + |SKY| + |SKZ|)^2.\end{aligned}$$

The maximum eigenvalue of the resulting matrix system, including both the viscous terms and the artificial dissipation term has been estimated as

$$\begin{aligned}\lambda_0 = &\sqrt{\lambda_I^2 + (4Re^{-1}SI/\Delta V + 16\epsilon K)^2} \\ &+\sqrt{\lambda_J^2 + (4Re^{-1}SJ/\Delta V + 16\epsilon K)^2} \\ &+\sqrt{\lambda_K^2 + (4Re^{-1}SK/\Delta V + 16\epsilon K)^2}\end{aligned} \tag{25}$$

where

$$\lambda_I = \frac{1}{2}\left[\hat{U}_I + \sqrt{\hat{U}_I^2 + \beta^2 SI}\right]$$

$$\lambda_J = \frac{1}{2}\left[\hat{U}_J + \sqrt{\hat{U}_J^2 + \beta^2 SJ}\right]$$

$$\lambda_K = \frac{1}{2}\left[\hat{U}_K + \sqrt{\hat{U}_K^2 + \beta^2 SK}\right]$$

and

$$\begin{aligned}\hat{U}_I =&|U| + |SIX\,(u_1 - z_1)| + |SIY\,(u_2 - z_2)| + |SIZ\,(u_3 - z_3)| \\ \hat{U}_J =&|V| + |SJX\,(u_1 - z_1)| + |SJY\,(u_2 - z_2)| + |SJZ\,(u_3 - z_3)| \\ \hat{U}_K =&|W| + |SKX\,(u_1 - z_1)| + |SKY\,(u_2 - z_2)| + |SKZ\,(u_3 - z_3)|\end{aligned}$$

Then the local time step has been computed from (23) with the maximum eigenvalue given by (25).

Profile Modification Algorithm

The principal steps of the optimization procedure are;

a) Choose an initial diffuser profile.
b) Generate a computational grid that conforms to the diffuser wall.
c) Obtain the steady state solution to the direct problem.

Third International Conference on Inverse Design and Optimization in Engineering Sciences
(ICIDES-III) Editor: G.S.Dulikravich, Washington D.C. October 23-25, 1991.

d) Obtain the steady state solution to the adjoint problem, by treating the required velocities as known from step (c).
e) Compute $\partial u_i/\partial n$ and $\partial z_i/\partial n$ from the solutions in steps (c) and (d) respectively. Choose a non-negative weighting function $\omega(s)$ and hence obtain $\rho(s)$ from (15).
f) Move nodes on the diffuser wall to be profiled along the outer normal direction by $\rho(s)$. The curve connecting the nodes after this movement represents the new diffuser profile.
g) Go to step (b) unless the change in diffuser pressure rise obtained from step (c) is smaller than a desired convergence parameter.

The iterative profile modification process is continued until the change in pressure rise is a small fraction of the total pressure rise. An alternate method is to continue the process until the value of $\rho(s)$ everywhere along the wall is less than a critical value. In step (e), the weighting function, $\omega(s)$, is chosen to be proportional to the arclength, s, along the diffuser wall measured from the diffuser entrance. This ensures that the entrance width is maintained constant but the exit width may vary with the diffuser profile. When shifting the diffuser wall to a new curve obtained from step (f) some care must be exercised since the curve is being redefined using only a finite number of discretely spaced points. Checks are performed on the location of points on the new curve to ensure that boundary nodes do not conglomerate or coalesce after their movement to a new position. Heuristic measures are also adopted to ensure that the appearance of small amplitude wiggles in the new profile are damped to some extent so as to prevent the growth and built up of numerical errors in the subsequent calculation

RESULTS AND DISCUSSION

Using the numerical solvers and the profile modification algorithm described above, optimum diffuser profiles have been obtained for a single diffuser length $L/W_1 = 3$ at Reynolds numbers Re=50, 100, 200 and 500. A sound speed, β^2, of 2 for the Navier-Stokes equations and 2.5 for the adjoint equations was used at all Reynolds numbers. The calculation at Re=200 (henceforth called the reference case) has been examined in particular detail to establish issues of convergence and accuracy.

The reference case was first examined for convergence of the profile modification algorithm. For this purpose, a computational grid of 61 nodes in the x and 31 nodes in the y directions is employed, both for the Navier-Stokes as well as the adjoint variable problem. Beginning with an initial shape the diffuser profile was obtained after each application of the shape modification algorithm. The initial profile and some of the intermediate profiles are shown in figure 3. The change in the profile shape is observed to be small between the fourth and the ninth iteration and the change was found to be insignificant after nine iterations. Hence the iterative process is stopped at the ninth iteration providing a reasonably converged optimum shape. The question of computational accuracy of the solvers and hence the accuracy of the optimum profile is addressed next.

The precise error due to a finite grid size on the optimum profile is difficult to determine since the actual optimum curve is not known apriori, nor are any other calculations or experimental data available. However one way to estimate the effects of the unavoidable truncation errors in a numerical calculation is to obtain the optimum diffuser profile using progressively finer grids until the there is no change with grid size. Once again the reference case of Re=200 was examined for this purpose using grids of 31 by 16, 61 by 31 and finally 121 by 61. The optimum profiles obtained using the three grids are shown in figure 4. The results show that the difference between the shapes is negligibly small, providing some evidence that at these grids the contribution of the truncation errors may not be significant. In view of this observation, a grid size of 61 by 31 is found to be a suitable compromise between accuracy and computational work for the results presented here.

In an earlier section we proposed that it was computationally desirable to replace some of the Dirichlet-type boundary conditions with Neumann-type conditions in both the Navier-Stokes and the adjoint equation solvers. To justify at least partially the validity of solving the modified numerical problem we must verify whether the optimum shapes obtained in this fashion do indeed satisfy the optimality condition, i.e. vanishing shear stress on the wall, arising from the analysis.

In figure 5 the wall shear stress normalized by the corresponding value for a straight duct, is shown for the optimum shape as well as at several intermediate stages of iteration. The wall shear stress for the optimum shape is found to be vanishingly small for all but 10 percent of the wall at the upstream end.

Third International Conference on Inverse Design and Optimization in Engineering Sciences
(ICIDES-III) Editor: G.S.Dulikravich, Washington D.C. October 23-25, 1991.

The shear stress distributions at intermediate iterations demonstrate a monotonous decrease towards the optimum values. Closer examination of the shear stress for the optimum and intermediate shapes at other Reynolds numbers confirm the same behavior as well. Hence the results obtained do provide some aposteriori justification for the boundary condition approximations made in the modified numerical problem.

Further justification is sought by examining the behavior of the objective function for the reference diffuser. The velocity averaged static pressure rise (i.e. the objective function defined by equation 2) is shown in figure 6 at successive iterations of the shape modification process. The objective function for this modified numerical problem is indeed found to increase with each application of the boundary movement suggested by equation (15). The area averaged static pressure rise through the reference diffuser also increases with with shape modification as seen in figure 6. These observations are found to be valid at calculations at other Reynolds numbers in the present study as well.

In addition to the reference case, calculation of the optimum diffuser profile was carried out at three other Reynolds numbers, Re= 50, 100 and 500. In figure 7, these profiles are shown for a diffuser of $L/W_1 = 3$ for a grid of 61 by 31. At lower Reynolds numbers the optimum diffuser profile permits a larger exit area to inlet area ratio as one would expect higher viscous effects to support greater diffusion without separation. The angle at which the diffuser profile departs at the upstream corner is difficult to compute accurately since the flow in that corner may not be accurately resolved. Nevertheless, the approximate angle decreases from 56 degrees to 19 degrees as the Reynolds number increases from 50 to 500. For the Reynolds number range in which numerical solutions are presented here, further refinement of the grid did not lead to any significant change in the optimum profile. This was not found to be true of computations at Reynolds numbers higher than 500.

To evaluate the performance of the optimum diffuser, a pressure recovery coefficient, C_p, is defined, which is the ratio of the static pressure rise of the optimum diffuser to the static pressure rise for an ideal diffuser (in potential flow) with the same W_2/W_1 ratio as the optimum diffuser. Note that the denominator of this ratio is independent of the actual profile between the upstream and downstream cross-sections of the diffuser. Using C_p as a parameter, the performance of the optimum diffuser is now compared with that of a straight walled diffuser with the same W_2/W_1 ratio at several different Reynolds numbers in the laminar regime. The C_p values of straight diffusers are found numerically using the Navier-Stokes solver on the straight walled geometry without any shape modification steps. As seen from figure 8, the C_p values for the optimum diffusers are always higher than those for straight diffusers.

In conclusion, the feasibility of shape optimization for incompressible laminar flows has been demonstrated. This approach may also be adopted to other domain optimization problems where the performance depends on the geometry of the component, and flow is governed by the viscous laminar flow (either compressible or incompressible) equations. It may also be possible to consider variations of the objective functions depending upon the design criterion of interest. All computational results presented in this paper were carried out either on an Intel 30386 33MHz microprocessor based machine or on a microVAX II workstation. The CPU times for these calculations are of the order of several hours. The theoretical framework as well as numerical solution code for the extension of the method to three-dimensional flow now exist and such flows are the subject of study by the authors at present.

The research reported in this paper is based upon work supported by the National Science Foundation under Grant No. CBT-87-10561.

BIBLIOGRAPHY

1. Cabuk, H. and Modi, V., "Shape Optimization Analysis: First- and Second-Order Necessary Conditions', *Optimal Control,- Applications and Methods*, **11**, 173–190 (1990).
2. Cabuk, H., Sung, C.-H. and Modi, V., "An Explicit Runge-Kutta Method for 3-D Internal Incompressible Flows", Submitted to AIAA J. (1991).
3. Chang, P. K., *Control of Flow Separation*, McGraw Hill Book Company, New York, 1976.
4. Chorin, A. J., "A Numerical Method for Solving Incompressible Viscous Flow Problems", *J. Comput. Physics* **2**, 12–26 (1967).
5. Giles, M., Drela, M. and Thompkins, W. T., "Newton Solution of Direct and Inverse Transonic Euler Equations", AIAA Paper 85-1530, Proc. AIAA 7th Computational Fluid Dynamics Conference,

Cincinnati, pp. 394–402 (1985).

6. Glowinski, R. and Pironneau, O., "On the Numerical Computation of the Minimum Drag Profile in Laminar Flow", *J. Fluid Mech.* **72**, 385–389 (1975).
7. Jameson, A., Schmidt, W. and Turkel, E., "Numerical Solutions of the Euler Equations by Finite Volume Methods Using Runge-Kutta Time-Stepping Schemes", AIAA Paper 81-1259, (June 1981).
8. Jameson, A.,"Aerodynamic Design via Control Theory", NASA ICASE Report 88-64, (November 1988).
9. Pironneau, O., "On Optimum Profiles in Stokes Flow", *J. Fluid Mech.* **59**, 117–128 (1973).
10. Pironneau, O., "On Optimum Design in Fluid Mechanics", *J. Fluid Mech.* **64**, 97–110 (1974).
11. Rizzi, A. and Eriksson, L.-E.,"Computation of Inviscid Incompressible Flow with Rotation", *J. Fluid Mech.* **153**, pp. 275-312 (1985).
12. Sung, C.-H., "An Explicit Runge-Kutta Method for 3D Turbulent Incompressible Flows", David W. Taylor Naval Ship Research and Development Center, Ship Hydromechanics Department Report DTNSRDC/SHD-1244-01, (July 1987).
13. Swanson, R. C. and Turkel, E., "A Multistage Time-Stepping Scheme for the Navier-Stokes Equations", AIAA Paper 85-35, (January 1985).
14. Thompson, J. F., Thames, F. C. and Mastin, C. W., "Automatic Numerical Generation of Body-Fitted Curvilinear Coordinate System for Field Containing any Number of Arbitrary Two-dimensional Bodies", *J. Comp. Phys.*, **15**, pp. 299–319 (1974).

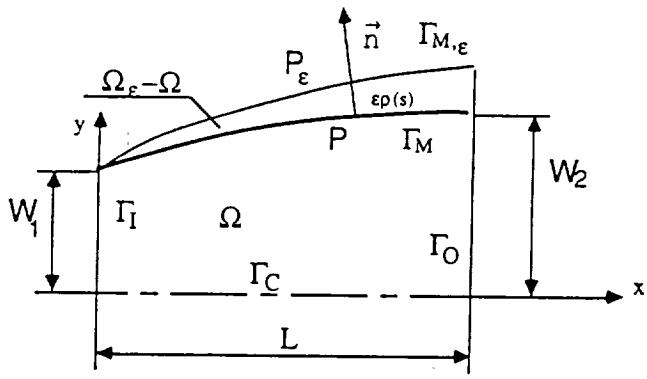

Figure (1) Schematic diagram of a plane diffuser. Flow enters at upstream boundary Γ_I and exits at the downstream boundary Γ_O. The wall to be shaped is Γ_M and symmetry line is Γ_C.

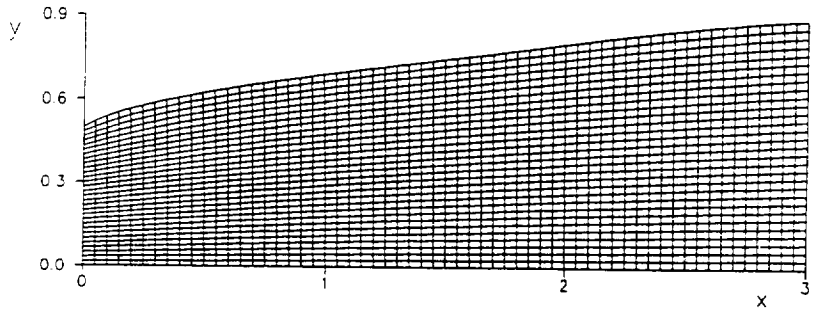

Figure (2) A typical computational grid for a plane diffuser obtained using the grid generation program. Grid size is 61 by 31. This was the domain for the optimum diffuser at Re=200 and $L/W_1 = 3$.

Third International Conference on Inverse Design and Optimization in Engineering Sciences
(ICIDES-III) Editor: G.S.Dulikravich, Washington D.C. October 23-25, 1991.

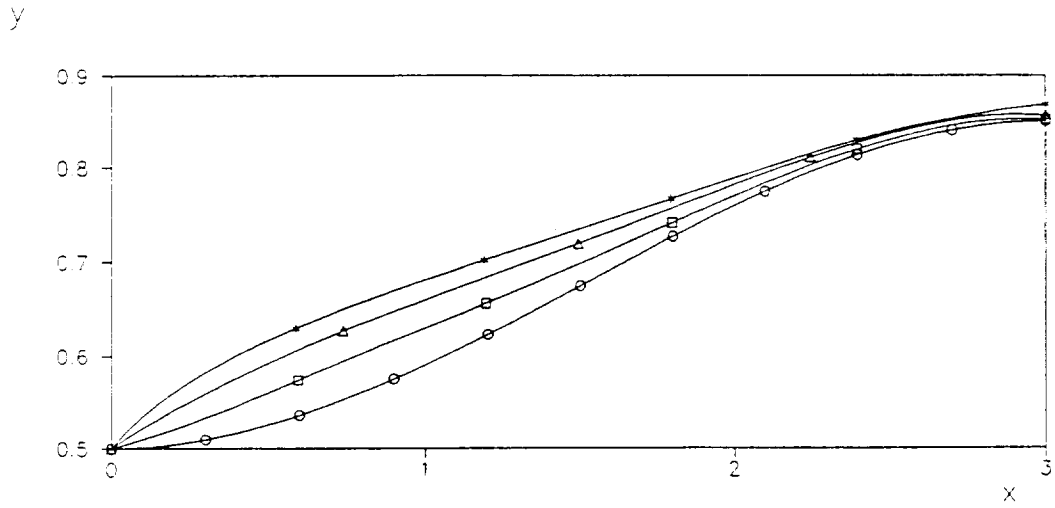

Figure (3) Profiles of a reference diffuser at successive iterations. The grid size is 61 by 31. ○ : Initial shape, □ : First iteration, △ : Fourth iteration, * : Ninth iteration.

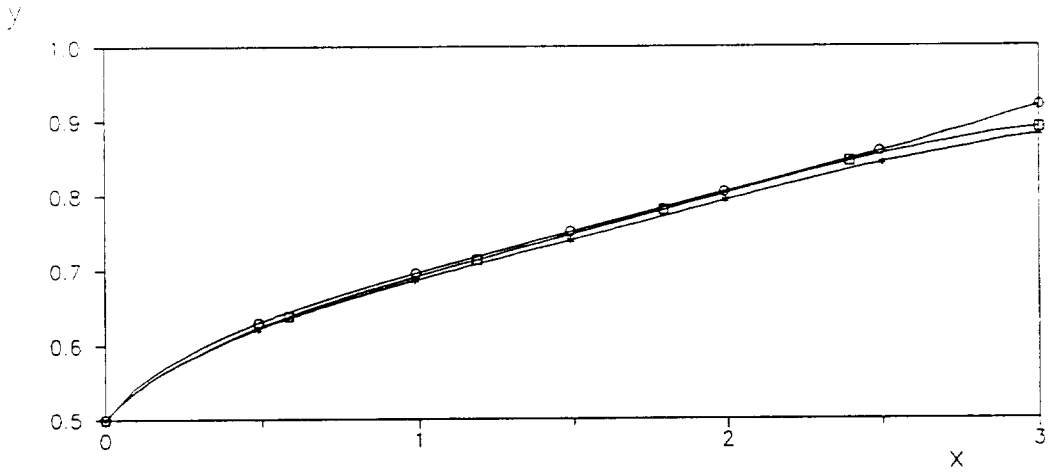

Figure (4) Effect of grid size on optimum profile of a reference diffuser. ○ : 31 by 16, □ : 61 by 31, * : 121 by 61.

Third International Conference on Inverse Design and Optimization in Engineering Sciences
(ICIDES-III) Editor: G.S.Dulikravich, Washington D.C. October 23-25, 1991.

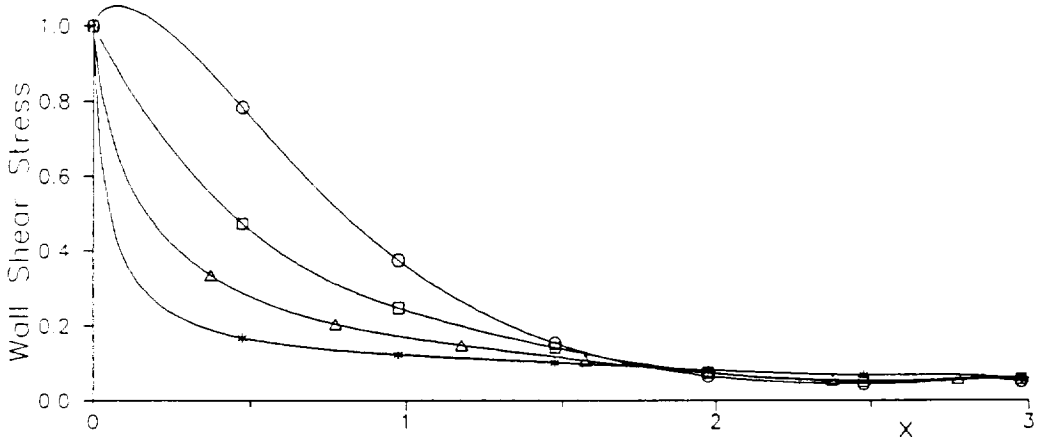

Figure (5) Normalized wall shear stress at successive iterations for a reference diffuser. The grid size is 61 by 31. ○ : Starting shape, ⊓ : First iteration, △ : Fourth iteration, * : Ninth iteration.

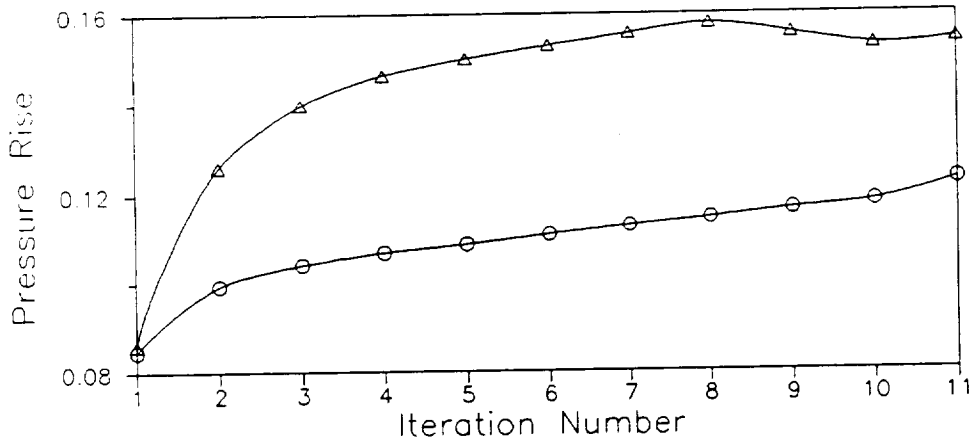

Figure (6) Static pressure rise through the reference diffuser at successive iterations. The grid size is 61 by 31. ○ : Area-averaged pressure rise, △ : Velocity-averaged pressure rise.

Third International Conference on Inverse Design and Optimization in Engineering Sciences
(ICIDES-III) Editor: G.S.Dulikravich, Washington D.C. October 23-25, 1991.

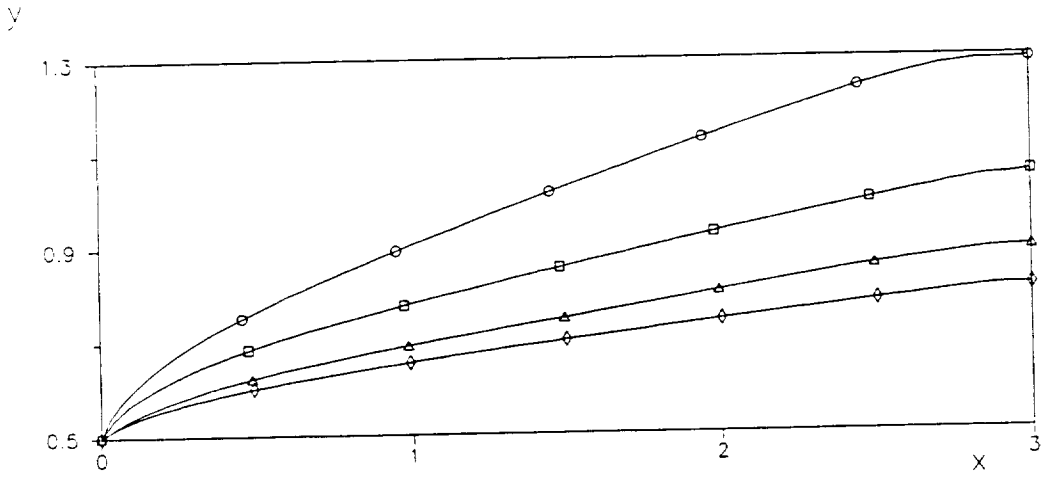

Figure (7) Optimum diffuser profiles at different Reynolds numbers for $L/W_1 = 3$. Grid size is 61 by 31. ○ : Re=50, □ : Re=100, △ : Re=200, ◇ : Re=500.

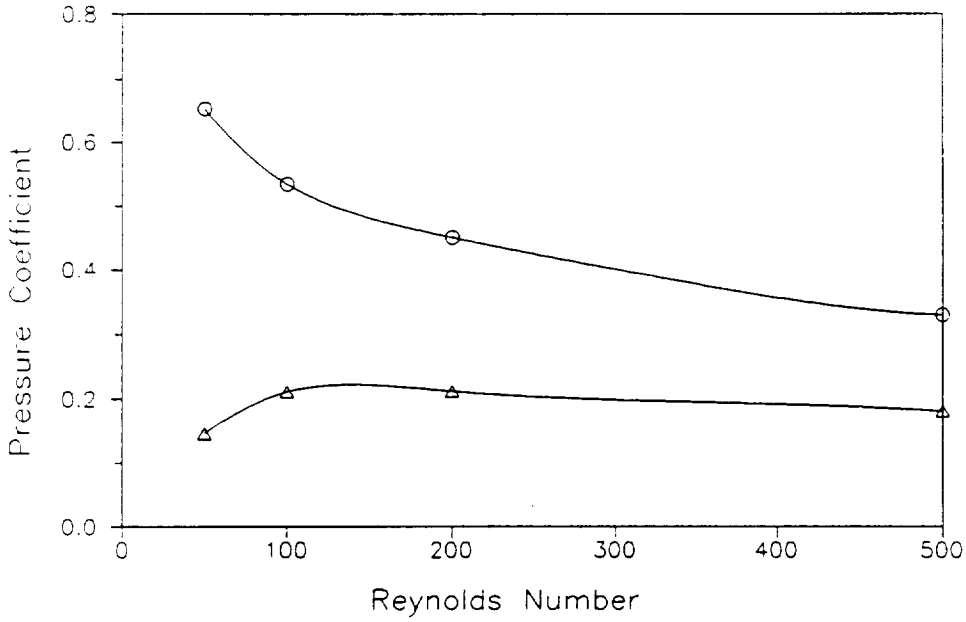

Figure (8) Variation of the pressure coefficient, C_p with Reynolds number for $L/W_1 = 3$. ○ : Optimal diffusers, △ : Straight diverging diffusers.